CHEMMEDCHEM

CHEMISTRY ENABLING DRUG DISCOVERY

Accepted Article

Title: Structure-Activity Relationships on Cynnamoyl Derivatives as Inhibitors of p300 Histone Acetyltransferase

Authors: Valentina Noemi Madia, Rosaria Benedetti, Maria Letizia Barreca, Liza Ngo, Luca Pescatori, Antonella Messore, Giovanni Pupo, Francesco Saccoliti, Sergio Valente, Antonello Mai, Luigi Scipione, Yujun George Zheng, Cristina Tintori, Maurizio Botta, Violetta Cecchetti, Lucia Altucci, Roberto Di Santo, and Roberta Costi

To be cited as: *ChemMedChem* 10.1002/cmdc.201700040

Link to VoR: http://dx.doi.org/10.1002/cmdc.201700040

A Journal of

ChemPubSoc Europe

WILEY-VCH

www.chemmedchem.org

10.1002/cmdc.201700040

Structure-Activity Relationships on Cynnamoyl Derivatives as Inhibitors of p300 Histone Acetyltransferase

Valentina Noemi Madia,[a] Rosaria Benedetti,[b] Maria Letizia Barreca,[c] Liza Ngo,[d] Luca Pescatori,[a] Antonella Messore,[a] Giovanni Pupo,[a] Francesco Saccoliti,[a] Sergio Valente,[a] Antonello Mai,[a] Luigi Scipione,[a] Yujun George Zheng,[d] Cristina Tintori,[e] Maurizio Botta,[e] Violetta Cecchetti,[c] Lucia Altucci,[b],[f] Roberto Di Santo,[a] and Roberta Costi *[a]

[a] Dr. V. N. Madia 0000-0002-5724-612X, Dr. L. Pescatori 0000-0003-4734-7856, Dr. A. Messore 0000-0003-0158-5816, Dr. G. Pupo 0000-0002-6011-0223, Dr.F. Saccoliti 0000-0002-9175-9199, Dr. S. Valente 0000-0002-2241-607X, Prof. A. Mai 0000-0001-9176-2382, Dr. L. Scipione 0000-0002-2006-7005, Prof. R. Di Santo 0000-0002-4279-7666, Prof. R. Costi 0000-0002-1314-9029
Dipartimento di Chimica e Tecnologie del Farmaco, Istituto Pasteur-Fondazione Cenci Bolognetti
"Sapienza" Università di Roma
P.le Aldo Moro 5, I-00185, Roma, Italy
E-mail: roberta.costi@uniroma1.it

[b] Dr. R. Benedetti, Prof. L. Altucci 0000-0002-7312-5387
Dipartimento di Biochimica, Biofisica e Patologia generale
Università degli Studi della Campania Luigi Vanvitelli
Vico L. De Crecchio 7, I-80138, Napoli, Italy

[c] Prof. M. L. Barreca 0000-0003-3530-5042, Prof. V. Cecchetti 0000-0001-8558-7004
Department of Pharmaceutical Sciences
University of Perugia
Via A. Fabretti 48, I-06123 Perugia, Italy

[d] Dr. L. Ngo, Prof. Y. G. Zheng 0000-0001-7116-3067
Department of Pharmaceutical and Biochemical Sciences
University of Georgia
Athens, Georgia, 30602, U.S.A.

[e] Dr. C. Tintori 0000-0002-6002-0332, Prof. M. Botta 0000-0003-0456-6995
Dipartimento di Biotecnologie, Chimica e Farmacia
Università degli Studi di Siena
Via Aldo Moro 2, I-53100, Siena, Italy

[f] Prof. L. Altucci 0000-0002-7312-5387
Istituto di Genetica e Biofisica, IGB 'Adriano Buzzati Traverso'
Via P. Castellino 111 I-80131, Napoli, Italy

Supporting information for this article is given via a link at the end of the document.

Abstract: Human p300 is a polyhedric transcriptional coactivator, playing a crucial role by acetylating histones on specific lysine residues. A great deal of evidences shows that p300 is involved in several diseases as leukemia, tumors and viral infection. Its involvement in pleiotropic biological roles and connections to diseases provide the rationale as to how its modulation could represent an amenable drug target. Several p300 inhibitors (HATi) have been described so far, but all suffer from low potency, lack of specificity or low cell-permeability, highlighting the need to find more effective inhibitors. Our cinnamoyl derivative, **RC 56**, was identified as active and selective p300 inhibitor, proving to be a good hit candidate to investigate the structure-activity relationship towards p300. Herein we describe the design, synthesis and biological evaluation of new HATi structurally related to our hit, investigating, moreover, the interactions between p300 and the best-emerged hits by means of induced fit docking and molecular dynamics simulations, gaining insight on the peculiar chemical features that influenced their activity toward the targeted enzyme.

Introduction

Described for the first time as adenoviral E1A-binding protein,[1] p300/CBP is a HAT (histone acetyltransferase) enzyme family together with other four families, including GNAT, MYST, nuclear receptor coactivators, and TBP-associated factor TAF_{II}.[2] p300 acts primarily as histone acetyltransferase, with the ability to transfer an acetyl group from acetyl-coenzyme A (acetyl-CoA) to the histone ε-NH_2 of lysine side chain, for remodeling chromatin to a relaxed superstructure. This modification results in the change of histone-DNA and histone-protein interactions. Histone acetylation can occur in promoter regions, where p300 acts as a transcription co-factor for a variety of nuclear proteins (including oncoproteins,[3] viral proteins[4] and tumor suppressor proteins[5]) or over large regions of chromatin, affecting global gene expression levels.[6] p300 substrates are not limited to histone proteins, but include more than 75 different proteins.[7] Noteworthy, p300 acetylation activity can be also addressed to viral proteins such as HIV-1 integrase, contributing significantly to viral replication.[8] Moreover, an extensive autoacetylation process occurs in an intermolecular fashion, regulating the activation state and the mediated transcriptional regulation of p300.[9]

By acetylating different substrates, p300 is implicated in a wide array of cellular processes, such as cell-cycle regulation,[10] differentiation[11] and DNA damage response,[12] and can promote opposite cellular outcomes such as proliferation and apoptosis.[13] Because of the biological importance of p300, the alteration in the gene sequence (mutation, chromosomal translocation and dysregulation) is correlated to many disease conditions, including cancer,[14] chronic neuropathic pain[15] and cognitive and neurodegenerative disorder.[16] Most recently, implication of p300 was also described in ventricular remodeling after myocardial infarction.[17]

p300 is characterized by highly conserved regions, which is possible to distinguish by four different functional domains: (i) a catalytic HAT domain, where the histone and proteins acetylation occurs; (ii) four recognized transactivation domains, that mediates protein-protein interactions with DNA-binding transcription factors and transcription machinery; (iii) the bromodomain that recognize histone acetylated tails and (iv) the cysteine-histidine-rich region. Recently, mutagenesis studies and resolution of structure of semi-synthetic heterodimeric p300 HAT domain in complex with Lys-CoA revealed the

catalytic mechanism of p300, where Tyr1467 and Trp1436 residues play a significant role in the acetylation reaction.[18] Tyr1467 guides and protonates the sulfur atom of acetyl-CoA, while Trp1436 orients the lysine side chain for the nucleophilic attack of the acetyl-CoA cofactor. More recently, the resolution of crystal structure of the p300 HAT domain bound to acetyl-CoA confirmed this hypothesis and gave insight for the design of p300 inhibitors.[19]

Due to the relevant role in different pathological conditions, HAT p300 is considered an amenable target and its modulation holds promise for future therapeutic strategies.[20] p300 inhibitors (HATi) so far described comprise natural compounds, some of them supplied from dietary plants, (i.e. anacardic acid,[21] curcumin,[22] garcinol,[23] epigallocatechin-3-gallate[24] and plumbagin[25]) and synthetic small molecules (i.e., Lys-CoA,[26] C646,[27] isothiazolones[28] and cinnamoyl compounds[29]) (Chart 1).

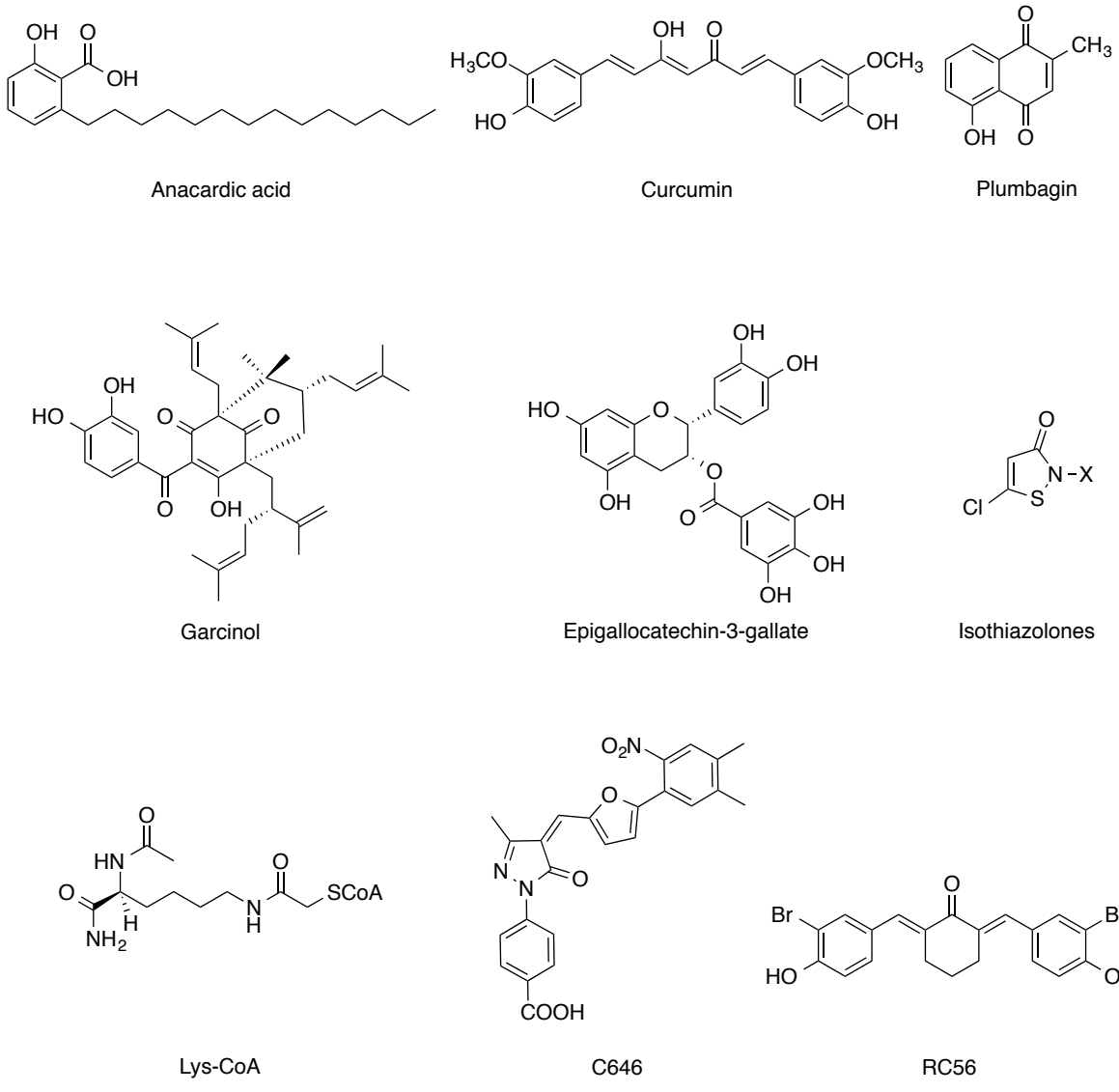

Chart 1. Chemical structures of known natural products and synthetic small molecules p300 inhibitors.

Nevertheless, in the field of HATi a huge investigation margin is left due to the necessity to find further inhibitors endowed with good pharmacokinetic and pharmacodynamic profiles, and to establish the exact inhibition mode towards p300. In the last decade our research group was involved in the identification of HATi[29] and among them **RC 56** [2,6-bis-(3-bromo-4-hydroxybenzylidene)cyclohexanone] (Figure 1) was identified as the most active and selective p300 inhibitor, showing cellular activity displayed by the down regulation of histone H3 acetylation level. Most recently **RC 56** was used as investigation tool to evaluate the acetylation level in H3K4 by p300 and the expression of multidrug resistance (*MDR1*) gene in drug-resistant and drug-sensitive breast carcinoma cell lines.[30] We considered **RC 56** a good hit candidate to investigate the structure-activity relationship towards p300. Herein we report the design of new HATi (**1a-s** and **2a**) addressing six modifications to the **RC 56** structure, which involved both the benzylidene moiety and the central cyclohexanone portion, so as to evaluate the role of the arylidene substituents, the central ring and the carbonyl group in inhibiting the enzymatic target. In particular, 1) the bromine atom in 3-position of the benzylidene portion was substituted with other atoms or groups: F (**1b**), Cl (**1c**), I (**1d**), methyl group (**1g**), hydroxyl group (**1e**), hydrogen atom (**1a**) and phenyl ring (**1f**); 2) the hydroxyl group in 4-position of the benzylidene portion was substituted with a bromine atom (**1h**); 3) a third substituent in 5-position of the benzylidene portion (Br, F, Cl) was introduced (**1i-j**); 4) the cyclohexanone was reduced to cyclohexanol (**2a**); 5) a carboxylic acid function was introduced in 4-position of the cyclohexanone ring (**1k-l**); 6) the cyclohexanone was substituted with 5-member ring (**1m**) or heterocycles: tetrahydro thiopyranone (**1n**) or piperidinone (**1o-s**). Thus, we report the synthesis and biological evaluation of the HATi **1a-s** and **2a** (Table 1). All the synthesized compounds were tested on recombinant p300 using an in vitro radiometric assay. Cell-based assays were performed with the most promising compounds to corroborate and strengthen the activities. Moreover, theoretical investigation of the interactions between p300 HAT and the best-emerged hits (i.e., **1d** and **1i**) was carried out by means of induced molecular modeling experiments.

Results and discussion

Chemistry. Bis-arylidene derivatives **1a-s** were obtained by microwave-assisted (**1a-j,m-n**) or acid catalyzed (**1k-l,o-s)** condensation of the appropriate five- or six-member cycle (see Table 1) with the appropriate benzaldehyde following a previously reported synthetic approach (Scheme 1).[29],[31] Derivative **2a** was obtained by reduction of the carbonyl group of **RC 56** to hydroxyl group in presence of lithium aluminum hydride (Scheme 2). All the benzaldehydes used as starting materials are commercially available, except **3d** and **3f**. Benzaldehyde **3d** was obtained as reported in literature,[32] while **3f** was synthesized by a Suzuki coupling reaction (Scheme 3).

10.1002/cmdc.201700040

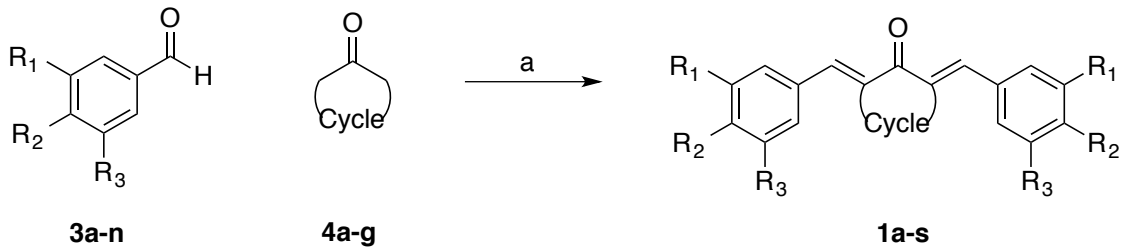

3a-n **4a-g** **1a-s**

[a] Reagents and conditions: a) **1a-j,m-n**: montmorillonite K-10, 100 W, 100 °C, 5 min; **1k-l,o-s**: HCl_g, CH_3COOH, room temp, 48 h.

Scheme 1.[a] Key synthetic step for the synthesis of the bis-arylidene derivatives **1a-s**.

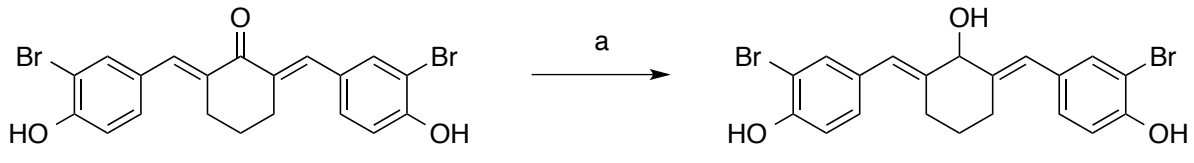

RC 56 **2a**

[a] Reagents and conditions: a) THF, $LiAlH_4$, 0 °C to room temp, 2h, 32%.

Scheme 2.[a] Synthesis of derivative **2a**.

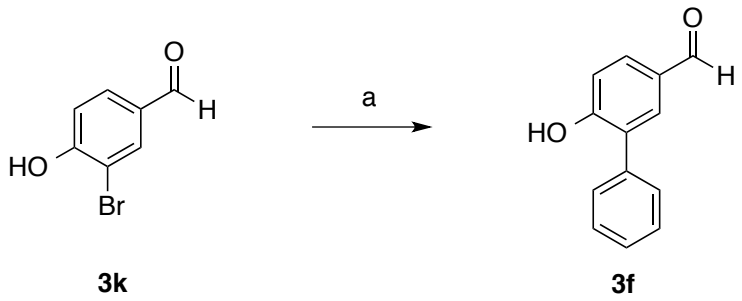

3k **3f**

[a] Reagents and conditions: a) phenylboronic acid, tetrakis(triphenylphosphine)palladium, $Ba(OH)_2 \cdot 8H_2O$, DME/H_2O, reflux, 4h, 32%.

Scheme 3.[a] Preparation of benzaldehyde **3f**.

Biological evaluation. The newly synthesized compounds **1a-s** and **2a** could be categorized according to the nature of the central cycle (cyclohexanone derivatives **1a-l**; cyclopentanone derivative **1m**; tetrahydrothiopyranone derivative **1n**; piperidinone derivatives **1o-s**; cyclohexanol derivative **2a**). All the compounds were tested against recombinant p300 (0.025

μM) using the standard filter binding assay. Conditions for this assay included 100 μM H3-20 peptide and 1 μM [^{14}C] Ac-CoA with a six-minute incubation at 30°C (Table 1). The activity of p300 was measured in the presence of individual compounds each at fixed concentration of 100 μM. The positive control contained no inhibitor. The activity of each inhibitor solution was compared with the positive control to calculate the percentage of p300 retaining activity (%), which was the quantitative representation of the potency of each inhibitor. IC_{50} values were further determined for those compounds showing less than 10% of p300 retaining activity at 100 μM (**1b-d,g,i,n**). **RC 56** was found previously by us to be a potent p300 inhibitor and thus was used as the reference compound. In this experiment **RC 56** revealed an IC_{50} value of 30.9 μM, six times greater than the one already reported.[29] The difference in the IC_{50} value of **RC 56** was attributed to altered assay conditions. In the previous study, GST-p300 HAT domain was used to acetylate a histone protein mixture with [^{14}C] Ac-CoA as cofactor. The acetylated products were visualized with phosphorimaging after SDS-PAGE separation. In the present study, a tag-free p300 was used as enzyme source and a high concentration of H3 peptide was used as substrate. The reaction yields were controlled under the initial reaction condition (product conversion typically is less than 20%).

Among the tested compounds, the cyclohexanone derivative **1i** was the most active compound showing complete inhibition to p300 activity at 100 μM. Its IC_{50} value was measured to be 2.3 ± 0.5 μM, fifteen times lower than **RC 56 (**30.9 ± 8.2 μM**)**. Of note, we also measured the IC_{50} of C646 at the same condition to be 3.6 ± 0.6 μM. C646 was regarded one of the most potent p300 inhibitor.[27] Therefore, the potency of **1i** is at the same level as C646.

Among the cyclohexanone derivatives **1a-l**, we discuss preliminary structure-activity relationship according to the substituents on the benzylidene portion. The substitution of the bromine atom of **RC 56** with hydrogen (**1a**), hydroxyl group (**1e**), phenyl ring (**1f**) resulted in the decrease of the inhibitory activity (% of residual acetylation of 28.6, 89.0, 92.2, respectively). The substitution of the bromine atom of **RC 56** with other halogen atoms (**1b-d**) as well as a methyl group (**1g**) led to compounds with good inhibitory activity. In fact, compounds **1b**, **1c** and **1g** showed IC_{50} values comparable with that of **RC 56** (IC_{50} values of 38.9 μM, 45.5 μM, 26.8 μM, respectively). Noteworthy, the substitution of bromine of **RC 56** with an iodine atom (**1d**) led to a five times more active compound (IC_{50} value of 8.1 μM). The introduction of a second bromine atom on the benzylidene portion (**1i**) generated the most potent compound (IC_{50} value of 2.3 μM), conversely the substitution of the two bromine atoms of **1i** with a fluorine and a chlorine atom (**1j**) decreased the activity (% of residual acetylation of 41.1). The biological data also suggested a key role of the hydroxyl groups on the benzene rings as highlighted by the comparison between **RC 56** (IC_{50} value of 30.9 μM) and derivative **1h** (% of residual acetylation of 85.1 at 100 mM).

The cyclohexanone and tetrahydrothiopyranone derivatives showed comparable activity (**RC 56** and **1n** IC_{50} values of 30.9 μM and 35.0 μM, respectively), while the substitution of the cyclohexanone ring with cyclopentanone (**1m**), piperidinone (**1o-s**) and cyclohexanol (**2a**) led to a decreasing in the inhibition potency (% of residual acetylation in the range of 12.5 and 128).

Among the piperidinone series featuring a 3,4-dihydroxybenzylidene substitution pattern, **1o-p,r**, the most active compound was the N-benzyl substituted piperidinone **1r**. In this series, the introduction of a benzyl group in 4-position of the

piperidinone ring (**1r**) increased the inhibition potency if compared with the unsubstituted counterpart (**1o**) (% of residual acetylation of 19.4 and 114, respectively). Moreover, comparing derivative **1r** with its analog **1s**, characterized by the substitution of the hydroxyl in 3-position of the benzylidene ring with a bromine atom, an activity decrease was observed (% of residual acetylation of 19.4 and 81.6, respectively). Interestingly, the replacement of the cyclohexanone of **RC 56** with a N-benzyl substituted piperidinone ring (**1s**), led to a decrease of inhibitory activity (% of residual acetylation of 81.6).

Interestingly, three compounds (**1l**,**o,q**) showed slight activation of p300 activity. This phenomenon is not unusual. In our previous study of anacardic acid analogs for HAT inhibition, we had similar observation that certain HAT inhibitors showed activating effect on p300 and PCAF activities.[33] The exact mechanism is not clear. Possibly, some inhibitor analogs can bind to HAT enzyme at a different conformation, thus working as an agonist instead of antagonist.

Table 1. p300 inhibitory activity of compounds **1a-s** and **2a** in enzyme assays.

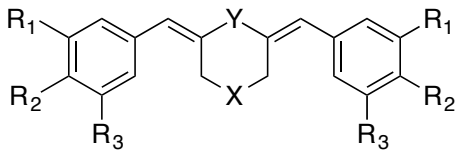

Cpd	X	Y	R_1	R_2	R_3	% retaining activity (100 μM)[a]	IC_{50}[b] (μM)
1a	CH_2	C=O	H	OH	H	28.6	
1b	CH_2	C=O	F	OH	H	6.3	38.9 ± 10.1
1c	CH_2	C=O	Cl	OH	H	7.7	45.5 ± 9.8
1d	CH_2	C=O	I	OH	H	5.8	8.1 ± 2.1
1e	CH_2	C=O	OH	OH	H	89.0	
1f	CH_2	C=O	Ph[c]	OH	H	92.2	
1g	CH_2	C=O	CH_3	OH	H	3.0	26.8 ± 11.2

10.1002/cmdc.201700040

1h	CH_2	C=O	Br	Br	H	85.1	
1i	CH_2	C=O	Br	OH	Br	0	2.3 ± 0.5
1j	CH_2	C=O	F	OH	Cl	41.1	
1k	CH_2COOH	C=O	COOH	OH	H	70.1	
1l	CH_2CH_2COOH	C=O	OH	OH	H	128	
1m	0	C=O	Br	OH	H	41.2	
1n	S	C=O	Br	OH	H	7.13	35.0 ± 12.3
1o[d]	NH	C=O	OH	OH	H	114	
1p[d]	$NHCH_3$	C=O	OH	OH	H	82.4	
1q[d]	$NHCH_2CH_3$	C=O	NO_2	OH	H	128	
1r[d]	$NHCH_2Ph$	C=O	OH	OH	H	19.4	
1s[d]	$NHCH_2Ph$	C=O	Br	OH	H	81.6	
2a	CH_2	CH-OH	Br	OH	H	12.5	
RC56	CH_2	C=O	Br	OH	H	0	30.9 ± 8.2
C646							3.6 ± 0.6

[a] The relative activity of p300 compared to the positive control which has no inhibitor present in the presence of 100 μM inhibitor; [b] IC_{50} (μM) determined from dose-response curves. The data represents the mean value of at least duplicates; [c] phenyl; [d] compounds tested as HCl salt.

Influence on the cell-cycle regulation.

Some of the compounds displaying activity against p300 were also tested in “cell-based assay” to verify their capability to modify cell cycle progression and induce cell death. Leukemic monoblast U937 cells were treated with 50 μM of each compound (as reported in Figure 1) for 30 hours. Next, cell cycle distribution and percentage of cell death were both analyzed. As shown in Figure 1, compound **1d** induced a weak G2 phase accumulation, whereas compounds **1a**, **1b**, **1f**, **1g** and **1n** caused an increase of cell number percentage in S phase.

Compounds **1b** and **1g** also showed a G1 block, coupled with induction of cell death (Figure1, panel B) greater than **RC56**. Compound **1i**, although did not change cell cycle distribution, compared to the ctr-untreated point, induced a weak cellular death (around 8.5%). It is interesting to note that for compounds **1b**, **1d**, **1g** and **1i** a strong correlation between the percentage of p300 inhibition (shown in Table 1) and the biological effect, reported here as inhibition of proliferation and induction of cell death (Figure 1, panel A and B), exists. The effect of compounds **1b** and **1g** seems to be very similar to **RC56**, showing a S phase accumulation and a value of p300 IC_{50} ranging from 38.9 ± 10.1 and 8.1 ± 2.1. However for both compound the percentage of cell death induction is greater than the one obtained with **RC56**.

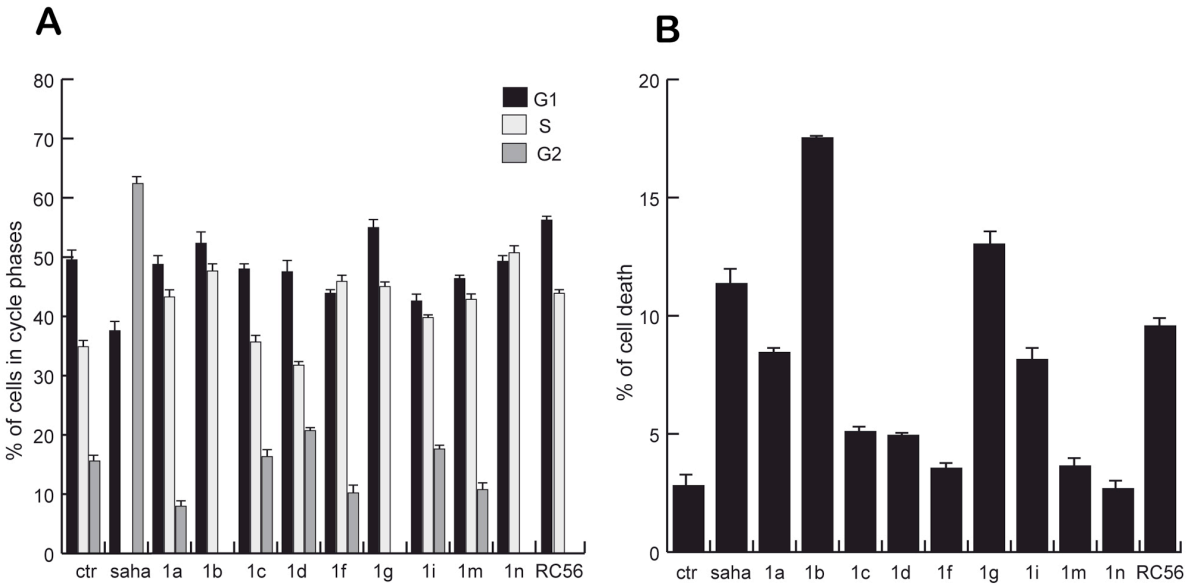

Figure 1. Cell cycle distribution; (A) % of cells in cell cycle phases and (B) apoptosis induction. SAHA was used as reference compound. Experiments were carried out as independent biological triplicates. Error bars show the standard deviation of triplicates.

Molecular modeling study. An in-depth theoretical investigation of the interactions between p300 HAT and the best-emerged hits (i.e., **1i** and **1d**) was carried out by means of induced fit docking (IFD), molecular mechanics-generalized

Born/Poisson Boltzmann surface area (MM-GBSA) experiments and Molecular Dynamics (MD) simulations. **RC 56** was analyzed as well as a reference compound.

Induced-fit docking experiments

Prior to docking, the compounds were built using the Schrödinger Maestro interface[34] and then submitted to the LigPrep utility,[35] which rapidly produces low energy 3D structures, taking into account ionization states, tautomerism, stereochemistry, and ring conformations at the desired pH. For our study, the default pH range of 6−8 was kept. This analysis suggested that three molecules could exist in a neutral (N), monoanionic (M) or dianionic (D) form. Given that, nine different structures were obtained: **RC 56**-N, **RC 56**-M and **RC 56**-D; **1i**-N, **1i**-M and **1i**-D; **1d**-N, **1d**-M and **1d**-D.

Then, docking experiments were carried out using the available crystal structure of p300 HAT–Lys-CoA complex (PDB ID 3BIY) and the IFD procedure,[36],[37],[38],[39],[40] which takes into account receptor flexibility upon ligand binding in an attempt to describe the inhibitor binding mode.

IFD of the nine structures into the Lys-CoA binding domain generated a number of protein/ligand complexes, and the best ten scoring poses for each ionization state were retained and further analyzed. A comparison between the IFD conformations for each ligand in the different N, M and D forms highlighted that all the docked positions could be clustered into two main distinct binding modes A and B (Figure 2), independently of the ionization state of the inhibitor.

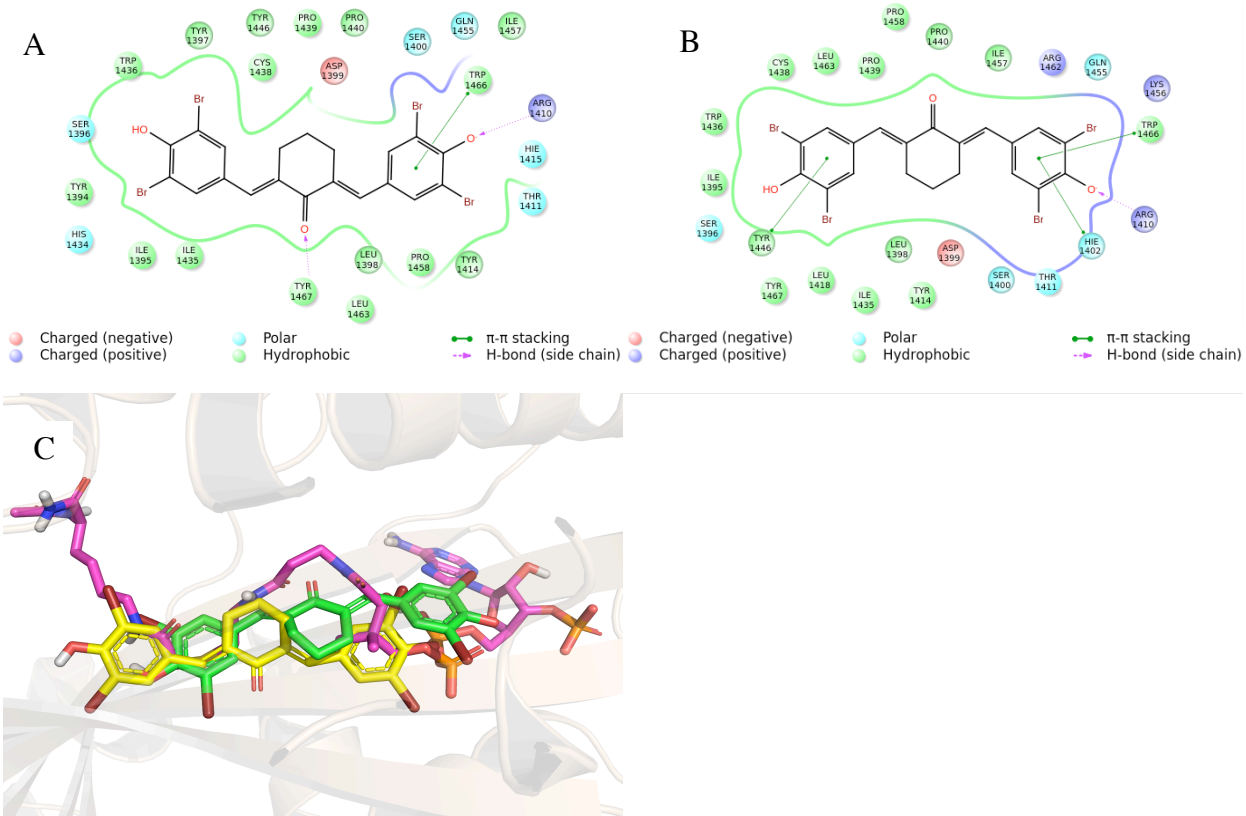

Figure 2. Alternative binding modes obtained for the cinnamoyl-based inhibitors at the p300 HAT domain. Figure 2A and 2B show a schematic representation of the interactions between the protein and **1i**, as representative inhibitor, for the binding mode A and B,

respectively. The superimposition of the two binding modes (A: yellow, B: green) and Lys-CoA (violet) substrate is represented as well (Figure 2C).

It is worth noting that a binding mode similar to A has been also predicted for compound **RC 56** by Devipriaya and Kumaradhas using a different docking protocol.[41]

In an attempt to gain a more accurate ranking of the ligand docking poses, the ligand-protein complexes were rescored using the MM-GBSA approach implemented in the Schrödinger's Maestro suite,[41] and the results are summarized in Table 2.

The binding pose A was predicted as the most favorable for both **RC 56** and **1d** inhibitors, although the lowest energy orientations were obtained for two different ionization states. Comparable MM-GBSA-dG values emerged for binding modes A and B of compound **1i**-M, suggesting that both poses could be reliable. It is also worth noting that for both binding modes the predicted binding energies reproduced the trend observed for the p300 HAT inhibitory activity, i.e. the most interesting compounds were in the order **1i**, **1d** and **RC 56**.

Table 2. MM-GBSA-DG values obtained for ligand-protein complexes selected by the IFD procedure.

Ligand in complex with HAT p300	Binding mode A	Binding mode B
	MM-GBSA-ΔG (Kcal/mol)	MM-GBSA-ΔG (Kcal/mol)
RC56-N	-135.53	-127.95
RC56-M	-126.98	-120.15
RC56-D	-113.05	-117.82
1d-N	-136.46	-131.57
1d-M	-147.15	-128.09
1d-D	-120.63	-112.70
1i-N	-145.42	-137.21
1i-M	-154.93	-154.47
1i-D	-136.29	-111.96

Molecular dynamics simulations.

In order to assess the stability of binding modes A and B previously identified for compound **1i**-M and to identify the most energetically favorable structure, the two ligand-p300 HAT complexes were submitted to 28 ns MD simulations in explicit solvent.

The superimposition between the final structures and the initial modeled structures showed that there were structural rearrangements within the binding site of both complexes (see Figure S2, Supporting Information). Analyzing the dynamical behavior of the complex between p300 HAT and the ligand with the binding mode A, we observed that the ligand did tend to move more internally into the pocket to maximize the interaction with the Arg1410 (more than 110% of occupancy), while the hydrogen bond with the Tyr1467 was lost and the interactions with this residue were later mainly of hydrophobic character. In its final pose the ligand established hydrophobic interactions with Ile1457, Leu1463, Leu1398, Trp1466, Tyr1414, Ile1395 and Ile1435 and made a weak hydrogen bond in turn with the carbonyl backbone of Ser1396 or Trp1436 (Figure 3A and 3C). On the other hand, a marked rearrangement of the residues of the binding site was observed for the complex B. In its final position the ligand made polar interactions with Arg1410 (over 70% of occupancy), with Tyr1467 (67% of occupancy), and with the carbonyl backbone of Trp1436 (occupancy around 22%) (Figure 3B and 3D). Hydrophobic contacts were also detected between **1i**-M and Trp1466, Tyr1414, Leu1398, Trp1436, Tyr1446, Ile1435 and Tyr1467. In this final complex, polar interactions as well as hydrophobic contacts were maximized. Accordingly, complex B resulted to be the most energetically favorable one in terms of free energy of binding between ligand and protein, being substantial the difference between the DG values of the two complexes (DDG of 9.47 Kcal/mol in favor of complex B that A).

The outputs of this study provide some useful information to aid the rational design of new cinnamoyl inhibitors of p300 HAT in the future.

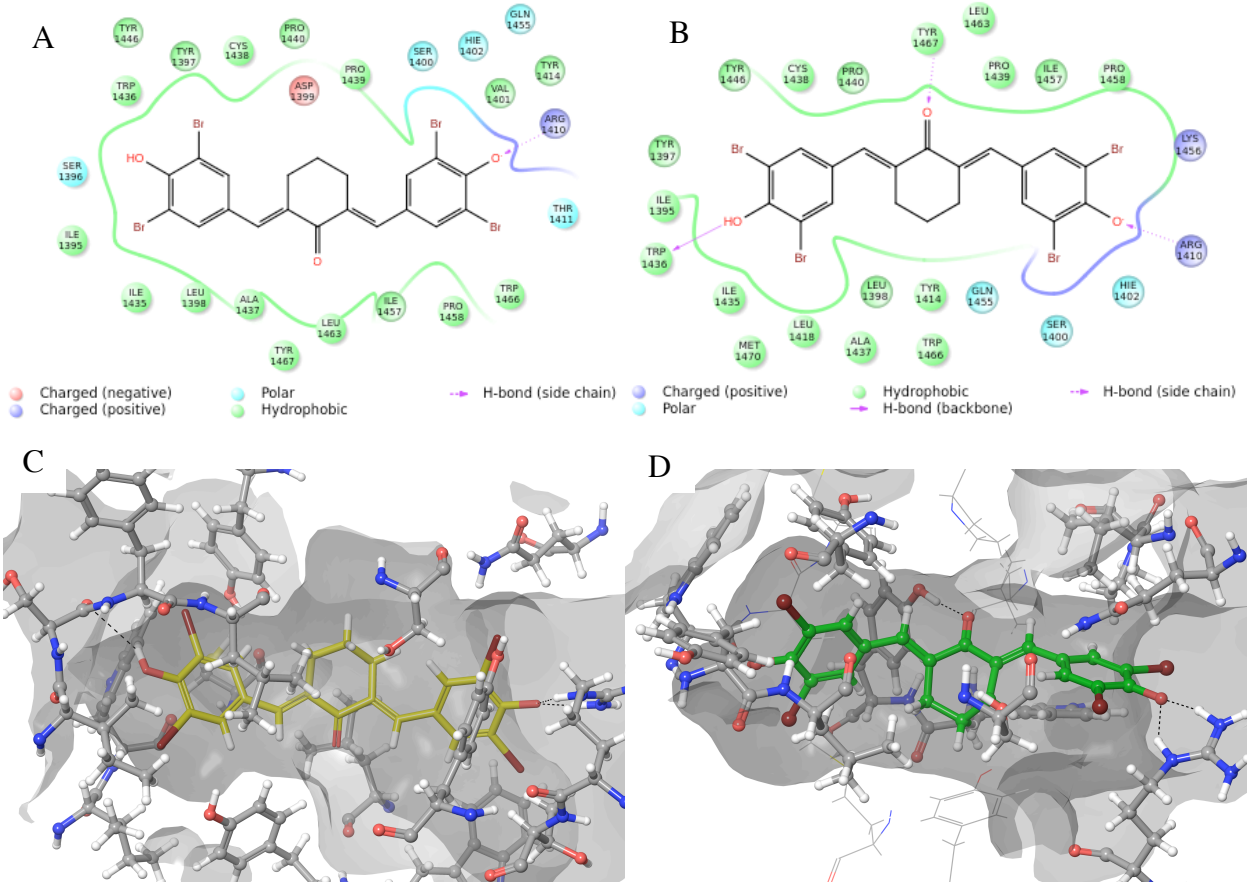

Figure 3. Minimized structures resulting from MD simulations of **1i**-M/p300 complexes A and B. Panels A and B show a 2D schematic representation of the interactions between the protein and **1i** for the binding mode A and B, respectively. Panels C and D provide the same information in a 3D perspective For the sake of clarity, only a few key residues are labeled and hydrogen-bonding interactions are represented by black dashed lines.

Conclusions

Herein we report a new series of cell-permeable cynnamoyl derivatives as inhibitors of p300 HAT addressing various structural modifications to our hit **RC 56**, involving both the benzylidene moiety and the central cyclohexanone portion. Among the tested derivatives, substituting the cyclohexanone with other central ring highlighted a decreasing trend in the inhibition potency (**1m**,**s**, **2a**), with the sole exception of the tetrahydrothiopyranone derivative (**1n**), characterized by a comparable activity in respect of **RC 56**. As regards the cyclohexanone derivatives, replacing the bromine atom of **RC 56** with other halogen atoms (**1b-d**) as well as a methyl group (**1g**) led to derivatives with IC_{50} values comparable with that of our hit. In particular, among them **1d** showed good inhibitory activity, proving to be five times more active (IC_{50} value of 8.1 μM) than reference compound, though data arising from cell-based assay showed higher percentage of cell death induction in leukemic monoblast cells for compounds **1b** and **1g**, even greater than the one obtained with **RC 56**. Noteworthy, the

cyclohexanone derivative **1i**, characterized by the introduction of a second bromine atom on the benzylidene portion, proved to be the most active compound with complete inhibition of p300 activity at 100 mM and IC_{50} value (2.3 ± 0.5 μM) fifteen times lower than **RC 56 (**30.9 ± 8.2 μM**)** and, notably, very similar to that of C646 (3.6 ± 0.6 μM), regarded one of the most potent p300 inhibitor. Furthermore, molecular modeling studies highlighted the main structural features involved in ligand-protein complex formation as for the key role played by the phenolate moieties in establishing a salt bridge with amino acidic residues at the active site, as stated by biological data (indeed, the substitution of hydroxyl groups with bromine atoms in derivative **1h** led to a remarkable decrease of the inhibition potency). Interestingly, two distinct binding modes within the p300 HAT domain, one for **RC 56** and **1d** and another for **1i**, were identified, suggesting that the introduction of a second bromine atom may cause a rearrangement of the inhibitor within the enzymatic binding site.

In conclusion, this study provided useful insights for future development of novel small molecules as p300 HAT inhibitors. In particular, the low micromolar inhibitor **1i** represents a very interesting compound whose further rational modifications might represent a line of inquiry for antitumor and antiviral vanguard chemotherapies.

Experimental section

Chemistry. General. Melting points were determined with a Büchi 530 capillary apparatus and are uncorrected. Compounds purity were always > 95% determined by high-pressure liquid chromatography (HPLC). HPLC analyses were carried out with Shimadzu LC-10AD VP CTO-10AC VP, using Discovery Bio Wide Pore C18 (10 cm x 4.6 mm, 3 mm) column. Infrared (IR) spectra were recorded on a Perkin-Elmer Spectrum-one spectrophotometer. ^{1}H NMR spectra were recorded on a Bruker AC 400 spectrometer. Merk silica gel 60 F_{254} plates were used for analytical TLC (thin layer chromatography). Developed plates were visualized by UV light. Column chromatographies were performed on silica gel (Merck; 70-230 mesh). Concentration of solution after reactions and extractions involved the use of a rotary evaporator operating at reduced pressure. Analytical results agreed to within ± 0.40% of the theoretical values. Dimethylsulfoxide-d_6 99.9% (code 44,139-2) and deuterochloroform 98.8% (code 41,675-4) of isotopic purity (Aldrich) were used. Solvents were reagent grade and, when necessary, were purified and dried by standard methods. Organic solutions were dried over anhydrous sodium sulfate (Merck).

Microwave irradiation experiments. Microwave reactions were conduced using a CEM Discover system unit (CEM. Corp., Matthews, NC). The machine consists of a continuous focused microwave-power delivery system with operator selectable power output from 0 to 300 W. The temperature of the contents of the vessel was monitored using a calibrated infrared temperature control mounted under the reaction vessel. All experiments were performed using a stirring option whereby the contents of the vessel are stirred by means of a rotating magnetic plate located below the floor of the microwave cavity and a Teflon-coated magnetic stir bar in the vessel.

All the final compounds **1a-s** and **2a** were synthesized according to the procedure reported in literature[29],[31] and described in Scheme 1. Spectroscopic, chemical and physical data of compounds **1a-b,e,g,i,l,n-r** are already described in

literature.[29],[31],[42] Spectroscopic, chemical and physical data of derivatives **1c-d,f,h,j-k,m,s** are reported below. Experimental procedure, yield (%), melting point (°C), recrystallization solvent, IR, ^{1}H NMR of derivatives **2a** and **3f** are reported below.

6-Hydroxy-[1,1'-biphenyl]-3-carboxaldehyde (3f). To a solution of **3k** (13.15 mmol) in DME (180 mL) phenylboronic acid (15.76 mmol), tetrakis(triphenylphosphine)palladium (0) (0.77 mmol), $Ba(OH)_2$ $8H_2O$ (19.73 mmol) and H_2O (22.6 mL) were added in turn. The reaction was stirred at reflux under argon atmosphere for 4 h. The reaction was quenched with water, extracted with ethyl acetate. The combined organic layers were washed with brine, dried over Na_2SO_4, filtered and evaporated under reduced pressure obtaining 6 g of crude product as yellow oil. Purification of crude product was performed by column chromatography on silica gel (chloroform/ethyl acetate 3:1 as eluent) obtaining 0.88 g of pure product as yellow oil (880 mg, 32% yield). Spectroscopic data as by reference.[43]

2,6-Bis(3-chloro-4-hydroxybenzylidene)cyclohexan-1-one (1c). Yield: 79 mg (40%); oil; ^{1}H NMR (400 MHz, [D_6]DMSO): δ=1.72-1.75 (m, 2H, CH_2), 2.85 (t, J_{CH2} = 8 Hz, 4H, CH_2), 7.04 (d, J_o = 8.4 Hz, 2H), 7.41 (d, J_o = 8.4, J_m = 1.8 Hz, 2H), 7.50 (s, 2H, =CH-), 7.54 (d, J_m = 1.8 Hz, 2H), 10.4 ppm (s br, 2H, OH); IR (KBr): ν= 3401 (OH), 1639 (C=O) cm^{-1}; Anal. Calcd for $C_{20}H_{16}Cl_2O_3$: C 64.02, H 4.30, Cl 18.89, found C 63.70, H 4.02, Cl 18.55.

2,6-Bis(4-hydroxy-3-iodobenzylidene)cyclohexan-1-one (**1d).** Yield: 98 mg (22%); mp: 183 °C; methanol; ^{1}H NMR (400 MHz, [D_6]DMSO): δ=1.71-1.74 (m, 2H, CH_2), 2.84 (t, J_{CH2} = 8 Hz, 4H, CH_2), 6.95 (d, J_o = 8.4 Hz, 2H), 7.43 (d, J_o = 8.4, J_m = 2.1 Hz, 2H), 7.48 (s, 2H, =CH-), 7.86 (d, J_m = 2.1 Hz, 2H), 11 ppm (s br, 2H, OH); IR (KBr): ν=3223 (OH), 1651 (C=O) cm^{-1}; Anal. Calcd for $C_{20}H_{16}I_2O_3$: C 43.04, H 2.89, I 45.47, found C 42.68, H 2.58, I 45.21.

2,6-Bis((6-hydroxy-[1,1'-biphenyl]-3-yl)methylene)cyclohexan-1-one (1f). Yield: 125 mg (42%); oil; ^{1}H NMR (400 MHz, [D_6]DMSO): δ=1.73-1.76 (m, 2H, CH_2), 2.91 (t, J_{CH2} = 8 Hz, 4H, CH_2), 7.05 (d, J_o = 8 Hz, 2H), 7.31 (d, J_o = 8 Hz, 2H), 7.42-7.46 (m, 8H), 7.86-7.89 (m, 6H), 10.1 ppm (s br, 2H, OH); IR (KBr): ν=3223 s br, 1664 (C=O) cm^{-1}; Anal. Calcd for $C_{32}H_{26}O_3$: C 83.82, H 5.72, found C 83.60, H 6.08.

2,6-Bis(3,4-dibromobenzylidene)cyclohexan-1-one (1h). Yield: 111 mg (36%); mp: 165 °C; benzene; ^{1}H NMR (400 MHz, [D_6]DMSO): δ=1.72-1.75 (m, 2H, CH_2), 2.86 (t, J_{CH2} = 8 Hz, 4H, CH_2), 7.43 (d, J_o = 8.3, J_m = 1.9 Hz, 2H), 7.54 (s, 2H, =CH-), 7.83 (d, J_o = 8.3 Hz, 2H), 7.91 ppm (d, J_m = 1.8 Hz, 2H); IR (KBr): ν=1661 (C=O) cm^{-1}; Anal. Calcd for $C_{20}H_{14}Br_4O$: C 40.72, H 2.39, Br 54.18, found C 40.37, H 1.99, Br 53.89.

2,6-Bis(3-chloro-5-fluoro-4-hydroxybenzylidene)cyclohexan-1-one (1j). Yield: 90 mg (22%); mp: 160-161 °C; toluene; ^{1}H NMR (400 MHz, [D_6]DMSO): δ=1.73-1.76 (m, 2H, CH_2), 2.86 (t, J_{CH2} = 8 Hz, 4H, CH_2), 7.42-7.47 (m, 6H), 10.97 ppm (s br, 2H, OH); IR (KBr): ν=1664 (C=O) cm^{-1}; Anal. Calcd for $C_{20}H_{14}Cl_2F_2O_3$: C 58.42, H 3.43, Cl 17.24, F 9.24, found C 58.71, H 3.22, Cl 17.61, F 9.49.

5,5'-((5-carboxy-2-oxocyclohexane-1,3-diylidene)bis(methanylylidene))bis(2-hydroxybenzoic acid) (1k). Yield: 131 mg (40%); mp: 170-173 °C; toluene; ^{1}H NMR (400 MHz, [D_6]DMSO): δ=2.80-2.82 (m, 2H, CH_2), 3.06-3.09 (m, 2H, CH_2), 7.06 (d,

J_o = 8.6 Hz, 2H), 7.61 (s, 2H, =CH-), 7.72 (d, J_o = 8.6, J_m = 1.2 Hz, 2H), 7.98 (d, J_m = 1.2 Hz, 2H), 12-13 ppm (s br, 2H, OH); IR (KBr): ν=3500-2500 (OH), 1650 (C=O) cm^{-1}; Anal. Calcd for $C_{23}H_{18}O_9$: C 63.02, H 4.14, found C 63.34, H 3.89.

2,5-bis((*E*)-3-bromo-4-hydroxybenzylidene)cyclopentan-1-one (1m). Yield: 110 mg (33%); mp: 154-156 °C; toluene; ^{1}H NMR (400 MHz, [D$_6$]DMSO): δ=2.99 (s, 4H, CH_2), 6.89 (d, J_o = 8.6 Hz, 2H), 7.42 (s, 2H, =CH-), 7.58 (d, J_o = 8.6, J_m = 1.2 Hz, 2H), 7.91 (d, J_m = 1.2 Hz, 2H), 10.2 ppm (s br, 2H, OH); IR (KBr): ν=3229 (OH), 1671 (C=O) cm^{-1}; Anal. Calcd for $C_{19}H_{14}Br_2O_3$: C 50.70, H 3.14, Br 35.50, found C 50.98, H 3.00, Br 35.29.

1-benzyl-3,5-bis((*E*)-3-bromo-4-hydroxybenzylidene)piperidin-4-one (1s). Yield: 94 mg (38%); mp: 180 °C; dioxane/diethyl ether; ^{1}H NMR (400 MHz, [D$_6$]DMSO): δ=3.42 (s, 4H, CH_2 piperidinone), 3.57 (s, 2H, CH_2Bz), 6.69 (d, J_o = 7.5 Hz, J_m = 1.2 Hz, 2H), 7.22-7.31 (m, 5H, Ph), 7.43 (d, J_o = 7.5, J_m = 1.2 Hz, 2H), 7.59 (s, 2H, =CH-), 8.26 (d, J_m = 1.2 Hz, 2H), 9.98 ppm (s br, 2H, OH); IR (KBr): ν=3225 (OH), 1674 (C=O) cm^{-1}; Anal. Calcd for $C_{21}H_{19}Br_2NO_3$: C 51.14, H 3.88, Br 32.40, N 2.84, found C 51.41, H 3.70, Br 32.79, N 2.99.

4,4'-(2-Hydroxycyclohexane-1,3-diylidene)bis(methanylylidene)bis(2-bromophenol) (2a). To a well stirred suspension of lithium aluminum hydride (50 mmol) in anhydrous THF (494 mL) cooled to 0 °C, a solution of **RC 56** (0.75 g, 1.63 mmol) in anhydrous THF (53 mL) was added drop wise. The reaction was then stirred at room temperature for 4 h. Crushed ice was added to the reaction mixture until the formation of hydrogen vapors was stopped. The produced aluminum hydroxide was filtered off by means a Buchner filter and the resulting solution was evaporated at reduced pressure obtaining 0.74 g of crude product. Purification of crude product was performed by column chromatography on silica gel (chloroform as eluent) obtaining 0.25 g of pure product as yellow oil (250 mg, 32% yield). ^{1}H NMR (400 MHz, [D$_6$]DMSO): δ=1.73-1.76 (m, 2H, CH_2), 2.84-2.87 (m, 4H, CH_2), 7.02 (d, J_o = 8.44 Hz, 2H), 7.41 (d, J_o = 8.50 Hz, 2H), 7.49 (s, 1H, =CH-), 7.68 (s, 1H=CH-), 10.79 ppm (s br, 1H, OH); IR (KBr): ν=3468 (OH), 3234 (OH) cm^{-1}; Anal. Calcd for $C_{20}H_{18}Br_2O_3$: C 51.53, H 3.89, Br 34.28, found C 51.69, H 4.13, 33.92.

Biological methods

Enzyme assays. The expression and purification of the tag-free recombinant human p300 HAT domain enzyme (residues 1287-1666) was done using the method developed by Cole's laboratory.[44] The standard filter binding assay was used to measure the acetyltransferase activity of p300 in the presence of various inhibitors. A histone H3 peptide containing the amino-terminal 20 residues (H3-20) was used as the substrate, and the concentration was set at 100 μM. 1 μM [^{14}C]-Ac-CoA as the acetyl donor. The reaction buffer contained 50 mM HEPES (pH 8), 1 mM EDTA, and 0.5 mM dithiothreitol (DTT). The reaction time was 6 minutes at 30°C. A 30-μL reaction volume comprised of inhibitor, peptide, and cofactor incubated for 5 minutes at 30°C followed by the addition of p300 (final at 0.025 μM). After 6 minutes of incubation the reaction was quenched by spreading 20 μL of the reaction mixture over a Whatman P81 filter disc. Once the filter discs were dried, they were washed three times with 50 mM $NaHCO_3$ (pH 9.0) and re-dried. Acetylated products were quantified using the MicroBeta2 (Perkin Elmer) after the addition of scintillation cocktail. The enzymatic reaction was controlled in the initial linear

phase, with a typical conversion yield of less than 20%. Each measurement was done at least in duplicate with errors less than 20%.

Cell-based assays. Drugs. SAHA (MERCK, Readington, NJ, USA) was dissolved in dimethylsulphoxide and used at 5 μM concentration.

Cell lines. U937 cells (ATCC) were cultured using standard procedures, in RPMI (Euroclone) supplemented with 10% FBS (Sigma) and 50 μg/ml penicillin-streptomycin and 2 mM glutamine.

Cell cycle Analysis. The cells were plated (2x105 cells/mL) and stimulated for 30 hours with compounds at 50 μM. Treated and untreated U937 cells were harvested and resuspended in staining solution containing RNaseA, PI (50 μg/ml), sodium citrate (0.1%), NP40 (0.1%) in cold PBS for 30 minutes in the darkness. Cell cycle distribution was assessed with a FACScalibur flow cytometer using the Cell Quest software (Becton Dickinson, Milan, Italy). ModFit LT version 3 Software (Verity, Topsham, ME, USA) was used for the analysis.

Cell death analysis. After stimulation with selected compounds for 30 hours at 50 μM, treated an untreated U937 cells were collected in 0.1% sodium citrate and 50 μg/ml PI. After 30 min incubation, the percentage of cells with sub-G1 DNA was analyzed with FACS (FACScalibur; BD Biosciences, San Jose, CA).

Molecular Modeling study. *Protein and Ligand Preparation*: The crystal structure of p300 HAT domain in complex with a bisubstrate inhibitor, i.e., Lys-CoA, was retrieved from the RCSB Protein Data Bank (PDB ID 3BIY)[45] and used as a target for the modeling studies. The inhibitor and the water molecules were deleted, and the Schrödinger Protein Preparation Wizard[46] was then used to obtain a satisfactory starting structure for docking studies. This facility is designed to ensure chemical correctness and to optimize a protein structure for further analysis. In particular, hydrogen atoms were added, and bond orders and charges were assigned; the orientation of hydroxyl groups on Ser, Thr and Tyr, the side chains of Asn and Gln residues, and the protonation state of His residues were optimized. Steric clashes were relieved by performing a small number of minimization steps, not intended to minimize the system completely. In our study, the minimization (OPLS force field) was stopped when the RMSD of the non-hydrogen atoms reached 0.30 Å. The analyzed compounds RC56, RC172 and RC175 were constructed using Maestro 9.9[34] and then submitted to the LigPrep module[35] using the default parameters.

Docking Studies: The IFD protocol,[36],[37],[38],[39] developed by Schrödinger was employed for prediction of ligand binding modes and concomitant structural changes in the p300 HAT receptor. The prepared protein structure was used to generate the receptor grid, which was centered on the crystallographic position of Lys-CoA substrate; afterwards, the simulations were run setting the “Extended Sampling” protocol and refining residues within 6 Å of all ligand poses. All the other parameters were left at the default values. Binding-free energy estimates were evaluated for the top docked complexes using MM–GBSA calculations.

Molecular Dynamics. Molecular Dynamic (MD) simulations have been performed through the use of AMBER 12 suite of programs (http://ambermd.org/)[47] and the ff03.r1 force field. An appropriate number of counter-ions were added to neutralize the system, and complexes were placed in an octagonal box of TIP3P water molecules. The distance between the box walls and the protein was set to 10 Å. MD runs were carried out with a protocol previously validated.[48],[49],[50] Before MD simulation, two stage of energy minimization were performed to remove bad contacts. In the first stage, we kept the protein fixed with a constraint of 500 kcal/mol and we minimized the positions of the water molecules. Then, in the second stage, we minimize the entire system, applying a constraint of 10 kcal/mol on the α carbons. MD trajectories were run using the minimized structure as starting input. Constant volume simulations were performed for 50 ps, during which time temperature was raised from 0 to 300 K using the Langevin dynamics method. Then, 150 ps of constant-pressure MD simulations were performed at 300 K in three steps of 50 ps each. During the three periods of this second stage, the α carbons were blocked with harmonic force constants of 10, 5, and 1 kcal/mol·Å, respectively. Finally a 28 ns MD simulation without restraint was run at a constant temperature of 300 K and a constant pressure of 1 atm. The root mean square deviations (RMSDs) of the α carbons were then calculated throughout the simulations with respect to the starting structure for both systems. After the first ns, both **1i**-M/p300 HAT complexes reached an equilibrium state, and stable RMSDs were detected during the remaining time of MD simulations (see Figure S1, Supporting Information).

Acknowledgments:

We wish to thank FIRB RBFR10ZJQT_003, EU (Blueprint High Impact project, n° 28251) and MIUR (PRIN 2012ZHN9YH; 20152TE5PK), EPIGEN (MIUR-CNR), AIRC (17217), POR Campania FESR 2007-2013-MOVIE (B25C13000240007) and COST EPICHEMBIO CM1406. Y. G. Z. was supported by AHA grant 12GRNT12070056 and NIH grant R01GM086717.

Keywords: Antitumor agents • Transferases • Medicinal chemistry • Drug discovery • Structure-Activity Relationships.

References:

[1] R. Eckner, M. E. Ewen, D. Newsome, M. Gerdes, J. A. DeCaprio, J. B. Lawrence, D. M. Livingston, *Genes Dev.* **1994**, *8*, 869-884.

[2] D. E. Sterner, S. L. Berger, *Microbiol. Mol. Biol. Rev.* **2000**, *64*, 435-459.

[3] a) A. C. Brown, V. Nair, M. Allday, *J. Virol.* **2012**, *86*, 1683-1695; b) B. Alberter, A. Ensser, *J. Virol*. **2007**, *81*, 2524-2530.

[4] a) M. T. Sáenz Robles, C. Shivalila, J. Wano, S. Sorrells, A. Roos, J. M. Pipas, *J. Virol.* **2013**, *87*, 13499-13509.

[5] S. J. Noh, M. J. Kang, K. M. Kim, J. S. Bae, H. S. Park, W. S. Moon, M. J. Chung, H. Lee, D. G. Lee, K. Y. Jang, *Pathology* **2013**, *45*, 574-580.

[6] S. K. Kurdistani, S. Tavazoie, M. Grunstein, *Cell*, **2004**, *117*, 721–733.

[7] J. H. Chen, Q. Li, *Epigenetics* **2011**, *6*, 957–961.

[8] Y. Zheng, X. Yao, *Viruses* **2013**, *5*, 1787-1801.

[9] M. Arif, G. V. P. Kumar, C. Narayana, T. K. Kundu, *J. Phys. Chem. B* **2007**, *111*, 11877–11879.

[10] N. G. Iyer, J. Xian, S-F. Chin, A. J. Bannister, Y. Daigo, S. Aparicio, T. Kouzarides, C. Caldas, *Oncogene* **2007**, *26*, 21–29.

[11] P-P. Wong, A. Pickard, D. J. McCance, *PLoS One* **2010**, *5*, e8369.

[12] a) R. K. Vempati, R. S. Jayani, D. Notani, A. Sengupta, S. Galande, D. Haldar, *J. Biol. Chem.* **2010**, *285*, 28553-28564; b) I.V. Getun, Z. Wua, m. Fallahi, S. Ouizem, Q. Liu, W. Li, R. Costi, W. R. Roush, J. L. Cleveland, P. R. J. Bois, *Cell Biol.* **2016**, 10.1128/MCB.00942-15.

[13] N. Gopalakrishna Iyer, S-F. Chin, H. Ozdag, Y. Daigo, D-E. Hu, M. Cariati, K. Brindle, S. Aparicio, C. Caldas, *Proc. Natl. Acad. Sci. U.S.A.* **2004**, *101*, 7386-7391.

[14] a) N. G. Iyer, H. Ozdag, C. Caldas, *Oncogene* **2004**, *23*, 4225-4231; b) F. Wang, C. B. Marshall, M. Ikura, *Cell. Mol. Life Sci.* **2013**, *70*, 3989-4008.
[15] X. Y. Zhu, C. S. Huang, Q. Li, R. M. Chang, Z. B. Song, W. Y. Zou, *Mol. Pain* **2012**, *8*, 84.
[16] L. M. Valor, J. Viosca, J. P. Lopez-Atalaya, A. Barco, *Curr. Pharm. Des.* **2013**, *19*, 5051-5064.
[17] K. Yasufumi, S. Yoichi, H. Koji, M. Tatsuya, *Bio. Pharm. Bull.* **2013**, *36*, 13-17.
[18] X. Liu, L. Wang, K. Zhao, P. R. Thompson, Y. Hwang, R. Marmorstein, P. A. Cole, *Nature* **2008**, *451*, 846−850.
[19] J. Maksimoska, D. Segura-Pena, P. A. Cole, R. Marmorstein, *Biochemisrty* **2014**, *53,* 3415-3422.
[20] F. J. Dekker, H. J. Haisma, *Drug Discov. Today* **2009**, *14,* 942-948.
[21] K. Balasubramanyam, V. Swaminathan, A. Ranganathan, T. K. Kundu, *J. Biol. Chem*. **2003**, *278*, 19134-19140.
[22] M. G. Marcu, Y-J. Jung, S. Lee, E-J. Chung, M. J. Lee, J. Trepel, L. Neckers, *Med. Chem.* **2006***, 2*, 169-174.
[23] S. A. Maddox, C. S. Watts, V. Doyère, G. E. Schafe, *PLoS One* **2013**, *8*, e54463.
[24] K-C. Choi, M. G. Jung, Y-H. Lee, J. Ch. Yoon, S. H. Kwon, H-B. Kang, M-J. Kim, J-H. Cha, Y. J. Kim, W. J. Jun, J. M. Lee, H-G. Yoon, *Cancer Res.* **2009**, *69,* 583-592.
[25] K. C. Ravindra, B. R. Selvi, M. Arif, B. A. A. Reddy, G. R. Thanuja, S. Agrawal, S. Kalyan Pradhan, N. Nagashayana, D. Dasgupta, T. K. Kundu, *J. Biol. Chem*. **2009**, *284*, 24453-24464.
[26] Y. Zheng, K. Balasubramanyam, M. Cebrat, D. Buck, F. Guidez, A. Zelent, R. M. Alani, P. A. Cole, *J. Am. Chem. Soc.* **2005**, *127*, 17182-17183.
[27] X-n. Gao, J. Lin, Q-y. Ning, L. Gao, Y-s. Yao, J-h. Zhou, Y-h. Li, L. Wang, L. A Yu, *PLoS One* **2013**, *8*, e55481.
[28] L. Stimson, M. G. Rowlands, Y. M. Newbatt, N. F. Smith, F. I. Raynaud, P. Rogers, V. Bavetsias, S. Gorsuch, M. Jarman, A. Bannister, T. Kouzarides, E. McDonald, P. Workman, G. W. Aherne, *Mol. Cancer Ther.* **2005**, *4*, 1521-1532.
[29] R. Costi, R. Di Santo, M. Artico, G. Miele, P. Valentini, E. Novellino, A. Cereseto, *J. Med. Chem.* **2007**, *50*, 1973-1977.
[30] M. Toth, I. M. Boros, E. Balint, *Cancer Sci.* **2012**, *103*, 659-669.
[31] R. Costi, R. Di Santo, M. Artico, S. Massa, R. Ragno, R. Loddo, M. La Colla, E. Tramontano, P. La Colla, A. Pani, *Bioorg. Med. Chem.* **2004***, 12*, 199-215.
[32] M. Azoulay, G. Tuffin, W. Sallem, J-C. Florent, *Bioorg. Med. Chem.* **2006**, *16*, 3147-3149.
[33] M. Ghizzoni, J. Wu, T. Gao, H. J. Haisma, F. J. Dekker, G. Y. Zheng, *Eur. J. Med. Chem*. **2012**, *47*, 337-344.
[34] Maestro, version 9.9, Schrödinger, LLC, New York, NY, 2014.
[35] LigPrep, version 3.1, Schrödinger, LLC, New York, NY, 2014.
[36] Schrödinger Suite 2014-3 Induced Fit Docking protocol; Glide version 6.4, Schrödinger, LLC, New York, NY, 2014; Prime version 3.7, Schrödinger, LLC, New York, NY, 2014.
[37] R. Farid, T. Day, R. A. Friesner, R. A. Pearlstein, *Bioorg. Med. Chem.* **2006**, *14*, 3160-3173.
[38] W. Sherman, T. Day, M. P. Jacobson, R. A. Friesner, R. Farid, *J. Med. Chem.* **2006**, *49*, 534-553.
[39] W. Sherman, H. S. Beard, R. Farid, *Chemi. Biol. Drug Des.* **2006**, *67*, 83-84.
[40] M. L. Barreca, N. Iraci, L. De Luca, A. Chimirri, *ChemMedChem.* **2009**, *4*, 1446-56.
[41] B. Devipriya, P. Kumaradhas, *Chem. Biol. Interact.* **2013**, *204*, 153-165.
[42] a) M. Artico, R. Di Santo, R. Costi, E. Novellino, G. Greco, S. Massa, E. Tramontano, M. E. Marongiu, A. De Montis, P. La Colla, *J. Med. Chem.* **1998**, *41*, 3948-3960; b) H. Ligeret, G. Barthélémy, S. Bouchard Doulakas, P-A. Carrupt, J-P. Tillement, S. Labidalle, D. Morin, *FEBS Lett.* **2004**, *569*, 37-42; c) M. A. Osman, A. Othman, M. A. Abd-Alla, *Polymer* **1992**, *33*, 52-56; d) A. Mai, D. Cheng, M. T. Bedford, S. Valente, A. Nebbioso, A. Perrone, G. Brosch, G. Sbardella, F. De Bellis, M. Miceli, L. Altucci, *J. Med. Chem.* **2008**, *51*, 2279-2290.
[43] J. Zhao, Q. Zhang, L. Liu, Y. He, J. Li, Q. Zhu, *Org. Lett.* **2012**, *14*, 5362-5365.
[44] P. R. Thompson, D. Wang, L. Wang, M. Fulco, N. Pediconi, D. Zhang, W. An, Q. Ge, R. G. Roeder, J. Wong, M. Levreno, V. Sartorelli, R. J. Cotter, P. A. Cole, *Nat. Struct. Mol. Biol.* **2004**, *11*, 308-315.
[45] X. Liu, L. Wang, K. Zhao, P. R. Thompson, Y. Hwang, R. Marmorstein, P. A. Cole, *Nature* **2008**, *451*, 846-850.
[46] Schrödinger Suite 2014-3 Protein Preparation Wizard; Epik version 2.9, Schrödinger, LLC, New York, NY, 2014; Impact version 6.4, Schrödinger, LLC, New York, NY, 2014; Prime version 3.7, Schrödinger, LLC, New York, NY, 2014.
[47] D. A. Case, T. A. Darden, T. E. III Cheatham, C.L. Simmerling, J. Wang, R. E. Duke, R. Luo, R. C. Walker, W. Zhang, K. M. Merz, B. Roberts, S. Hayik, A. Roitberg, G. Seabra,J. Swails, A. W. Götz, I. Kolossváry, K. F. Wong, F. Paesani, J. Vanicek, R. M. Wolf, J. Liu, X. Wu, S. R. Brozell, T. Steinbrecher, H. Gohlke, Q. Cai, X. Ye, J. Wang, M. J. Hsieh, G. Cui, D. R. Roe, D. H. Mathews, M. G. Seetin, R. Salomon-Ferrer, C. Sagui, V. Babin, T. Luchko, S. Gusarov, A. Kovalenko, P. A. Kollman, AMBER 12, University of California, San Francisco, 2012.
[48] C. Tintori, N. Veljkovic, V. Veljkovic, M. Botta, *Proteins* **2010**, *78*, 3396-3408.
[49] T. Tuccinardi, F. Manetti, S. Schenone, A. Martinelli, M. Botta, *J. Chem. Inf. Model.* **2007**, *47*, 644–655.
[50] C. Granchi, S. Roy, S. A. De Simone, I. Salvetti, T. Tuccinardi, A. Martinelli, M. Macchia, M. Lanza, L. Betti, G. Giannaccini, A. Lucacchini, E. Giovannetti, R. Sciarrillo, G. J. Peters, F. Minutolo, *Eur. J. Med. Chem.* **2011**, *46*, 5398-5407.

Inhibiting p300 HAT in cancer therapy

10.1002/cmdc.201700040

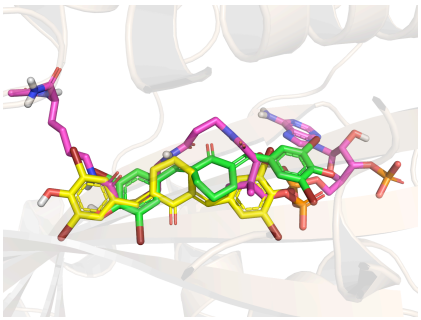

HAT is an attractive anticancer target. Several HAT inhibitors have been identified, but all exhibit low potency or pharmacodynamics limits. We report the design and synthesis, along with biological evaluation and theoretical investigation, of potent and selective cinnamoyl compounds, highlighting the peculiar features required to develop effective HATi.